Rapid Communications

Spatial structure of quasilocalized vibrations in nearly jammed amorphous solids

Masanari Shimada,[1,*] Hideyuki Mizuno,[1] Matthieu Wyart,[2] and Atsushi Ikeda[1]
[1]*Graduate School of Arts and Sciences, The University of Tokyo, Tokyo 153-8902, Japan*
[2]*Institute of Physics, EPFL, CH-1015 Lausanne, Switzerland*

(Received 30 April 2018; published 20 December 2018)

The low-temperature properties of amorphous solids are widely believed to be controlled by the low-frequency quasilocalized modes. However, what governs their spatial structure and density is unclear. We study these questions numerically in very large systems as the jamming transition is approached and the pressure p vanishes. We find that these modes consist of an unstable core and a stable far-field component. The length scale of the core diverges as $p^{-1/4}$ and its characteristic volume diverges as $p^{-1/2}$. These spatial features are precisely those of the anomalous modes that are known to cause the boson peak in the vibrational spectra of weakly coordinated materials. From this correspondence, we deduce that the density of quasilocalized modes must follow $g_{\rm loc}(\omega) \sim \omega^4/p^2$, which is in agreement with previous observations. Thus, our analysis demonstrates the nature of quasilocalized modes in a class of amorphous materials.

DOI: 10.1103/PhysRevE.98.060901

Introduction. The low-temperature $T \lesssim 1$ K properties of amorphous solids are universal and markedly different from those of crystals [1,2]. Their specific heat increases linearly with T and their thermal conductivity increases as T^2 [1,2]. To explain these observations, Anderson *et al.* [3] and Phillips [4] proposed the famous two-level systems model, which was later extended to the soft potential model [5–7]. This theory postulates that amorphous solids have the low-frequency, quasilocalized vibrational modes in addition to phonons, which can cause double-well structures in the energy landscape. The universal properties of amorphous solids can be explained in terms of the quantum tunneling of these two-level systems and their interactions with phonons.

However, the current theory is phenomenological and does not specify the nature of these localized modes, which remains a matter of debate [8,9]. This led to a substantial effort to characterize quasilocalized modes numerically. Schober and Laird detected them in molecular dynamics simulations in a model amorphous solid that was composed of soft spheres [10] and later extended to Lennard-Jones glasses [11–13], vitreous silica [14], amorphous silicon [15], and weakly jammed solids [16]. It was demonstrated that these modes (i) have strong anharmonicity [14,16], in accordance with the assumption of the soft potential model [5–7]; (ii) display a vibrational density of states (vDOS) $g_{\rm loc}(\omega)$ that follows a power law, $g_{\rm loc}(\omega) \propto \omega^4$ [17–21], where ω is the frequency, which is in agreement with previous arguments for disordered bosonic systems [9,22]; (iii) consist of core and far-field components that decay algebraically in space if they are not strongly hybridized with phonons [18,23]. This decay is sufficiently rapid for their participation ratio to scale as $1/N$, as for truly localized modes, where N is the number of particles; (iv) are suppressed if the prestress is removed [20,24]; (v) and play an important role in mechanical failure under a load [25–27] and in the structural relaxation near the glass transition [28,29]. Interestingly, their characteristic frequency appears to increase rapidly as that transition is approached, in concert with a local measure of elastic stiffness [30]. Despite these recent advances, understanding what determines the nature and density of these modes remains a challenge.

In this Rapid Communication, we seek to answer these questions by studying the spatial architecture of these modes and how it is affected by the proximity of the jamming transition. This transition is reached in finite-range repulsive interacting particles as the pressure, which is denoted as p, vanishes [31,32]. Excess modes with respect to the Debye density of states, which is called the boson peak [2] and is a well-known property of the vibrational spectra of amorphous solids, is singular at that point. The associated modes, which are called "anomalous" in this context, have been characterized in detail; they lead to a flat vibrational spectrum above a characteristic frequency, which is denoted as $\omega_* \sim p^{1/2}$ [32–43]. By considering very large systems, we can study localized soft modes, even close to the jamming transition. We find that these modes consist of an unstable core and a stable far-field component and that the length scale of the core diverges as $p^{-1/4}$ and its characteristic volume diverges as $p^{-1/2}$. These features are precisely those of the anomalous modes at the boson peak frequency if the prestress is removed (which corresponds to removing all forces between interacting particles). Thus, our analysis supports that localized soft modes are anomalous modes that are shifted to lower frequencies via the destabilizing effect of the prestress. From this result, we deduce that the density of quasilocalized modes must satisfy $g_{\rm loc}(\omega) \sim \omega^4/p^2$, which is in agreement with previous observations [20]. Finally, we discuss how our result on the nature of localized modes generalizes to other glasses.

Methods. We used monodisperse, three-dimensional packings of particles with mass m that interact through a

*masanari-shimada444@g.ecc.u-tokyo.ac.jp

finite-range, harmonic potential (see Ref. [20] for details):

$$\phi(r) = \frac{\epsilon}{2}\left(1 - \frac{r}{\sigma}\right)^2 H(\sigma - r), \tag{1}$$

where σ is the particle diameter, ϵ is the characteristic energy, and $H(r)$ is the Heaviside step function. Length, mass, and time are measured in units of σ, m, and $\sqrt{m\sigma^2/\epsilon}$, respectively. The packings were generated by quenching random configurations to mechanically stable inherent structures via the FIRE algorithm [44] and removing the rattlers that have less than three contacting neighbors (almost all rattlers have no contacting neighbors). We prepared 16 packings for pressure $p = 0.05, 0.02, 0.01, 0.005$, 15 packings for $p = 0.002$, and 8 packings for $p = 0.001$. The system size (number of particles) is fixed at $N = 1\,024\,000$; we also analyzed systems with $N = 256\,000$ and confirmed that there is no system size dependence in the analyzed quantities.

Next, we analyze the vibrational modes of these packings. We denote the kth eigenvector as $\boldsymbol{e}^k = [\boldsymbol{e}_1^k, \boldsymbol{e}_2^k, \cdots, \boldsymbol{e}_N^k]$ and its eigenvalue as $\lambda^k = (\omega^k)^2$, where ω^k is its eigenfrequency. The eigenvectors are orthonormalized. After removing three translational zero modes, eigenmodes are sorted in ascending order of their eigenvalues: $\omega^1 < \omega^2 < \cdots < \omega^{3N-3}$. Then, for a specified mode k, the indices of particles are sorted in descending order of their norms: $|\boldsymbol{e}_1^k| > |\boldsymbol{e}_2^k| > \cdots > |\boldsymbol{e}_N^k|$. Particles are labeled differently for each mode.

To focus only on the quasilocalized modes and exclude any effects that are due to hybridization with phonons, we selected the vibrational modes that are located below the lowest frequency of phonons in our analysis, as follows [18]. First, we estimated the width of the band of the lowest-frequency phonon via the same method as Ref. [23]. Then, we fitted the peak of the vDOS of the lowest-frequency phonon to the Gaussian function and obtained the mean frequency, which is denoted as ω_1, and the standard deviation, which is denoted as $\Delta\omega_1$, of the band. Finally, we estimated the width of the band to be $3\Delta\omega_1$ and selected only the vibrational modes that satisfy $\omega^k \in [0, \omega_1 - 3\Delta\omega_1]$ in our analysis. In the main text, we denote the average over all the analyzed modes as $\langle\bullet\rangle_k$.

Results. Figure 1 shows the lowest-frequency modes of the systems at the highest ($p = 0.05$) and lowest ($p = 0.001$) pressures (three samples for each pressure). Each arrow indicates an eigenvector component $\boldsymbol{e}_i^k$; only those that are larger than 1% of the largest component are shown. These modes present a core in which the displacement is large and heterogeneous, whose size appears to increase as the pressure decreases.

To characterize the vibrational motions of particles in these modes, we calculate the contribution δE_i^k of particle i to the energy of the mode k, which must satisfy $\lambda^k/2 = \sum_i \delta E_i^k$ [45]:

$$\delta E_i^k = \frac{1}{4}\sum_{j\in\partial i}\left[\left(u_{ij}^{\parallel}\right)^2 - \frac{f_{ij}}{r_{ij}}\left(u_{ij}^{\perp}\right)^2\right], \tag{2}$$

where ∂i labels the set of particles that interact with particle i, $u_{ij}^{\parallel} = (\boldsymbol{e}_i^k - \boldsymbol{e}_j^k)\cdot\hat{\boldsymbol{r}}_{ij}$ is the relative displacement between i and j parallel to the bond ij of direction $\hat{\boldsymbol{r}}_{ij}$, $u_{ij}^{\perp} = \sqrt{|u_{ij}^{\parallel}|^2 - [(\boldsymbol{e}_i^k - \boldsymbol{e}_j^k)\cdot\hat{\boldsymbol{r}}_{ij}]^2}$ is the perpendicular component of that relative displacement, and $f_{ij} = -d\phi(r_{ij})/dr$ is the contact force. Force f_{ij} is always positive in this system, and packings are called unstressed when $f_{ij} = 0$ [35]. Next, we calculate the average energy $\langle\delta E_i^k\rangle_k$ of the ith particle with the ith largest displacement over all the quasilocalized modes that we obtain at a specified pressure.

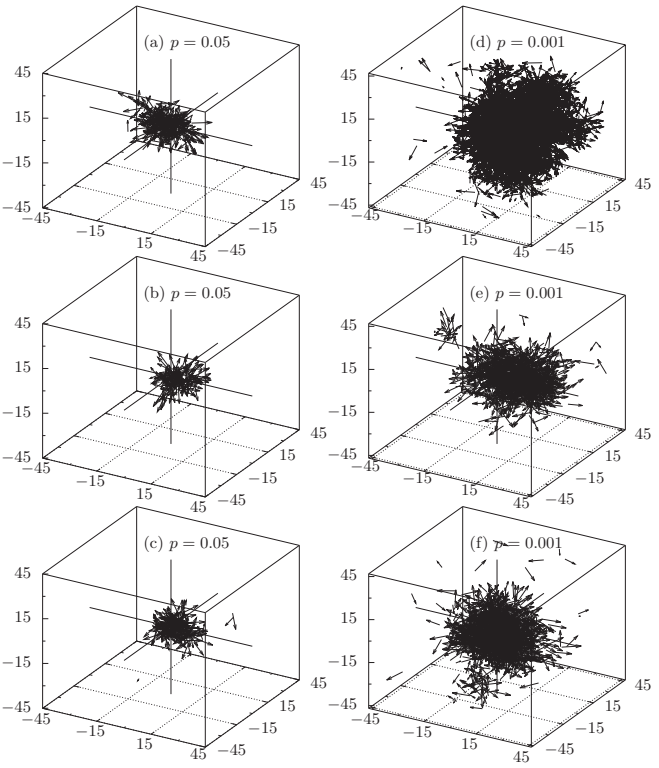

FIG. 1. Vibrational displacement field in the quasilocalized vibrations at (a)–(c) high ($p = 0.05$) and (d)–(f) low ($p = 0.001$) pressures (three samples for each pressure). We show the particles' vibrational displacements (denoted by arrows) that are larger than 1% of the largest vibrational displacement, and the particle with the largest displacement is positioned at the center of the box. These modes are chosen from the lowest-frequency modes in each configuration.

In Fig. 2, we plot $\langle\delta E_i^k\rangle_k$ vs the average norms $\langle|\boldsymbol{e}_i^k|\rangle_k$. We find that the larger the norm, the lower the energy. In particular, particles in the core (particles with large norm) have *negative* energies [46]. This result implies that the perpendicular motion, namely, $u_{ij}^{\perp}$, is highly dominant there, since it is the only negative contribution to the energy according to Eq. (2) and $f_{ij}/r_{ij} \ll 1$ near the jamming transition. It is generally known that vibrational motions in the anomalous modes that are responsible for the boson peak [35,42], nonaffine displacements under global deformations near the jamming transition [47], and the transition between double-well potentials [48] are also largely perpendicular to bonds.

To study the spatial distribution of δE_i^k, we define the radial energy distribution function:

$$\delta E(r) = \left\langle \frac{\sum_i \delta E_i^k \delta(r - r_i)}{\sum_i \delta(r - r_i)} \right\rangle_k, \tag{3}$$

where r_i is the distance of particle i from the particle with the lowest energy. This function measures the average energy

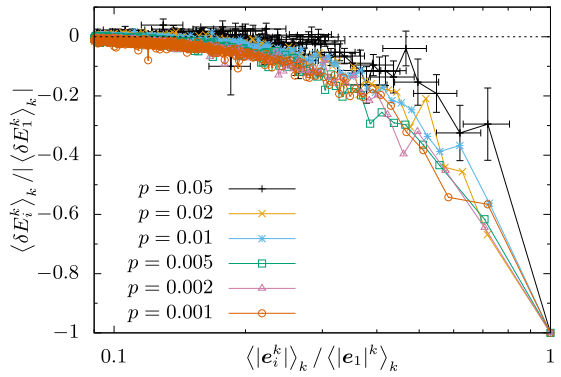

FIG. 2. The average energy versus the average norm of each particle. Both axes are normalized by the values of the particle with the largest displacement. Error bars are shown only for pressure $p = 0.05$; the other errors are comparable. The symbols are connected by lines to guide the eye.

of the particles at distance r from the center of the localized mode. Figure 3(a) shows $\delta E(r)$ for various values of p. For the moment, we focus on data that are far from jamming, which correspond to $p = 0.05$ (black line). We observe that

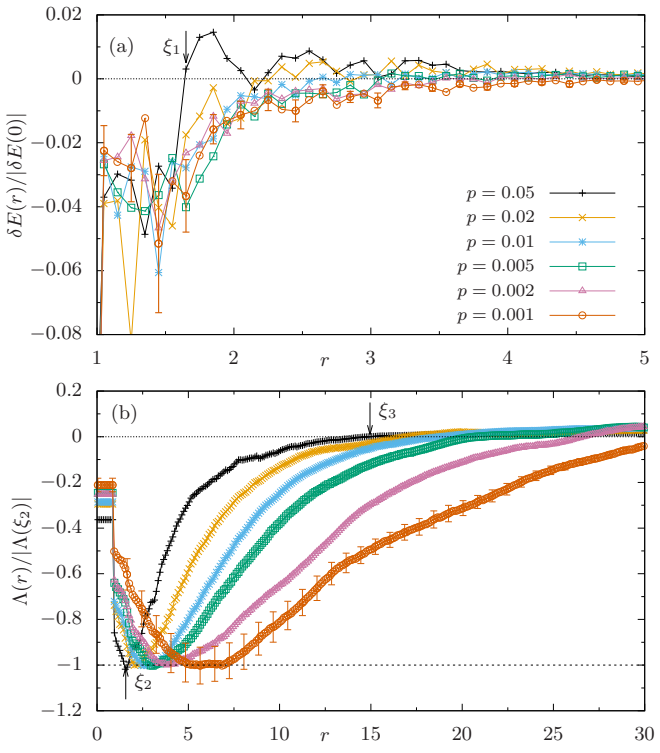

FIG. 3. (a) Radial energy distribution functions $\delta E(r)$, which are normalized by their values at the origin, for various values of pressure p. We define the length ξ_1 where the functions initially become positive and plot it for $p = 0.05$. (b) Integrated radial energy distribution functions $\Lambda(r)$, which are normalized by their minimum values. We also defined the length ξ_2 at which the functions attain their minimum value and ξ_3 at which the functions first become positive. For visibility in (a) and (b), we show error bars only for $p = 0.001$; the other error bars are comparable.

$\delta E(r)$ is negative up to a length scale, which we denote as ξ_1; here, $\xi_1 \approx 1.5$. For $r \gtrsim \xi_1$, $\delta E(r)$ is a positive quantity and decays rapidly with distance, as expected from the decay of the displacements. Thus, ξ_1 characterizes the size of the unstable core of the localized modes, which is stabilized by its far-field components that correspond to $r > \xi_1$. Note that in previous work [18], the size of the core was measured from the decay profile of the far-field components in several structural glasses.

Then, we calculate the integrated radial energy distribution function, which is defined as

$$\Lambda(r) = \left\langle \sum_{r_i \leqslant r} \delta E_i^k \right\rangle_k . \tag{4}$$

$\Lambda(r)$ corresponds to the average energy that the localized modes would have if the system were cut at a distance r from the center of the localized mode. It follows that $\lim_{r\to\infty} \Lambda(r) = \langle \lambda^k \rangle_k / 2$. There is a direct link between $\Lambda(r)$ and $\delta E(r)$:

$$\Lambda(r) \approx \int d\boldsymbol{r}' \rho G(r') \delta E(r'), \tag{5}$$

where ρ is the number density and $G(r)$ is the radial distribution function. [Note that this is an approximate relation because the normalization by the number of particles is performed before the averaging for $\delta E(r)$, but not for $\Lambda(r)$.]

$\Lambda(r)$ are shown for various pressures in Fig. 3(b). Again, we focus on $p = 0.05$ for the moment (black line). According to Eq. (5), the negativity of $\delta E(r)$ at small distances results in the negativity of $\Lambda(r)$ at small r, which must attain its minimum value at distance ξ_1, which is defined above. For $r > \xi_1$, $\Lambda(r)$ gradually increases and becomes positive at a distance that we denote as ξ_3. Here, $\xi_3 \approx 15$, which is tenfold larger than the core size of ξ_1. In practice, this result demonstrates that even far from the jamming transition, cutting the system around a localized mode at a large distance $r < 15$ (and imposing external forces at the particles at the boundary to maintain the force balance) would not lead to a stable system; the localized mode would still be unstable and rearrangements would necessarily occur. The emerging physical picture for quasilocalized modes is that of a core that has an elastic instability that is caused by prestress (a phenomenon that is similar to the well-known buckling instability) [35,45], but is stabilized by the surrounding elastic medium. This situation is similar to confined thin sheets, where buckling can be prevented by adhering the system to a surrounding stabilizing elastic medium [49].

Now, we study how the architectures of the quasilocalized modes depend on the proximity to the jamming transition. We consider three lengths from the observables that are introduced above: We recall that ξ_1 is defined as the length at which $\delta E(r)$ becomes positive. We define ξ_2 as the length at which $\Lambda(r)$ attains its minimum value, which must satisfy $\xi_1 \approx \xi_2$ according to Eq. (5). Lastly, ξ_3 is smallest r for which $\Lambda(r)$ becomes positive. ξ_1, ξ_2, and ξ_3 are indicated in Figs. 3(a) and 3(b) by arrows for $p = 0.05$. The pressure dependences of ξ_1, ξ_2, and ξ_3 are shown in Fig. 4(a), which are consistent

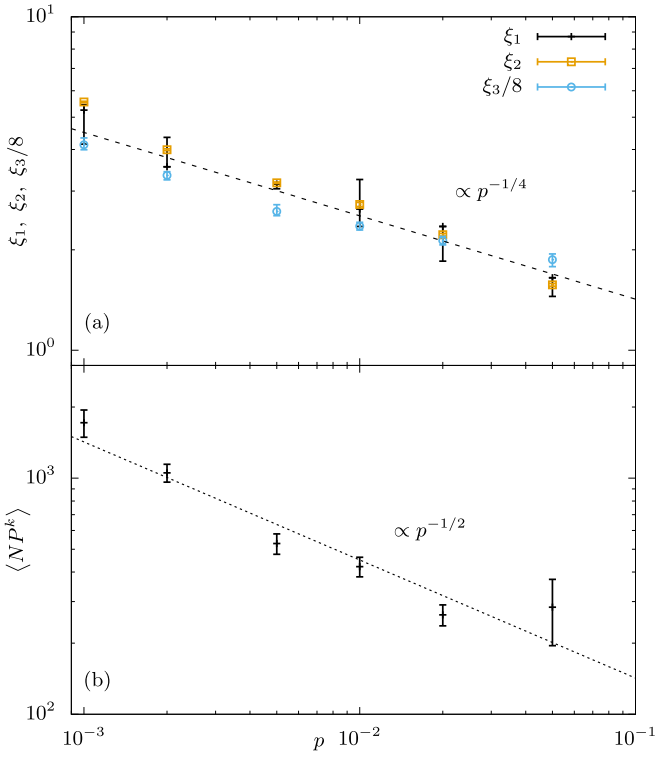

FIG. 4. (a) The pressure dependences of three lengths, namely, ξ_1, ξ_2, and ξ_3, which are defined in the main text and Fig. 3. Since ξ_3 is much larger than the other two lengths, we present ξ_3 divided by 8. The dashed line indicates the power-law dependence of $\propto p^{-1/4}$. (b) The pressure dependence of the volume. The dotted line indicates the dependence of $\propto p^{-1/2}$.

with the following power-law dependence:

$$\xi_1, \xi_2, \xi_3 \propto p^{-1/4}. \tag{6}$$

Therefore, the quasilocalized modes become further extended as $p \to 0$ and their characteristic length scale diverges at the jamming transition. Note that the errors of ξ_1 and ξ_3 in Fig. 4 were estimated from the errors of $\delta E(r)$ and $\Lambda(r)$. ξ_2 was decided by fitting a quadratic function around the minimum of $\Lambda(r)$, and errors with this fitting are shown in the figure.

Another characterization of these modes is their participation ratio, which is expressed as $P^k = N^{-1}[\sum_i (\boldsymbol{e}_i^k \cdot \boldsymbol{e}_i^k)^2]^{-1}$. The quantity NP^k is an estimate of the number of particles that are involved in the mode k [11,12,14]. We define the average volume of the localized modes as $V \equiv \langle NP^k \rangle_k$, whose dependence on p is shown in Fig. 4(b). Once again, we observe a singular behavior near the jamming transition, which is consistent with

$$V \propto p^{-1/2}. \tag{7}$$

Discussion. The scaling results, which are expressed as Eqs. (6), and (7), support that the quasilocalized modes are the anomalous modes that are responsible for the boson peak in these systems, whose properties we now recall. Near the jamming transition, the density of the vibrational modes exhibits a flat spectrum $g(\omega) \sim \omega^0$ at frequencies $\omega > \omega_*$ [32,33], where $\omega_* \propto p^{1/2}$. Anomalous modes at ω_* [whose characteristic number must vary as $N(p) \sim g(\omega_*)\omega_* \sim p^{1/2}$] are spatially extended but can be characterized by a finite correlation length that diverges at the jamming transition as $\ell_c \propto p^{-1/4}$ [33,36,39], which is a length scale that also characterizes the response to a local perturbation [50–52]. These results can be derived via effective medium calculations [38,40]. Recently, a variational argument was introduced to show that these modes can be localized on a length scale l_c and a characteristic volume $V \propto p^{-1/2}$ [43] without significantly affecting their frequency scale. We remark that $V \propto p^{-1/2}$ differs from l_c^d, where d is the spatial dimension, due to the algebraic decay of the mode magnitude in space. Thus, the architecture that we discovered for quasilocalized modes is fully consistent with that of anomalous modes.

This correspondence can be used to explain how the density of quasilocalized modes depends on the distance to the jamming transition. The characteristic number of anomalous modes obeys $N(p) \sim p^{1/2}$; according to this scaling law, there is one anomalous mode in this frequency scale for every volume V. Let us assume that a finite fraction of these modes become quasilocalized. According to general arguments [22], their density must follow $g_{\rm loc}(\omega) \sim c(p)\omega^4$. This requires that

$$\int_0^{\omega_*} g_{\rm loc}(\omega) d\omega \sim \omega_* \sim \frac{1}{V}. \tag{8}$$

It follows that $c(p) \sim V^{-1}\omega_*^{-5} \propto p^{-2}$, as demonstrated numerically [20]. Our approach provides a rationale as to why the density of quasilocalized modes explodes near the jamming transition.

Overall, our work suggests that quasilocalized modes correspond to the anomalous modes that are known to control the boson peak in finite-range interacting systems. Although this correspondence is most stringently tested near the jamming transition, where both objects display singular properties, we expect it to hold away from the jamming transition as well. If so, our conclusion should hold for Lennard-Jones glasses, where the boson peak can also be interpreted in terms of the distance to a jamming transition (however, it cannot vanish due to long-range interactions) [53], and in chalcogenide glasses and silica, where jamming corresponds to the point at which the covalent network becomes rigid [40,54]. Since experimental glasses are obtained from supercooled liquids that are annealed for a long time [55], it would be important to study the effects of the annealing in the future.

We thank H. Yoshino, E. Lerner, L. Manning, M. Popovic, T. DeGeus, W. Ji, F. Zamponi, and P. Derlet for discussions. This work was supported by JSPS KAKENHI Grants No. JP17K14369, No. JP17H04853, and No. JP16H04034; the Swiss National Science Foundation under Grant No. 200021-165509; and the Simons Foundation under Grant No. 454953 (M.W.). The numerical calculations were partly performed in the Research Center for Computational Science, Okazaki, Japan.

[1] R. C. Zeller and R. O. Pohl, Phys. Rev. B **4**, 2029 (1971).
[2] W. Phillips, *Amorphous Solids: Low-Temperature Properties*, Topics in Current Physics (Springer-Verlag, Berlin, 1981).
[3] P. W. Anderson, B. I. Halperin, and C. M. Varma, Philos. Mag. **25**, 1 (1972).
[4] W. A. Phillips, J. Low Temp. Phys. **7**, 351 (1972).
[5] V. G. Karpov, M. I. Klinger, and F. N. Ignat'ev, Zh. Eksp. Teor. Fiz. **84**, 760 (1983).
[6] U. Buchenau, Y. M. Galperin, V. L. Gurevich, and H. R. Schober, Phys. Rev. B **43**, 5039 (1991).
[7] U. Buchenau, Y. M. Galperin, V. L. Gurevich, D. A. Parshin, M. A. Ramos, and H. R. Schober, Phys. Rev. B **46**, 2798 (1992).
[8] C. C. Yu and A. J. Leggett, Comments Condens. Matter Phys. **14**, 231 (1988).
[9] V. L. Gurevich, D. A. Parshin, and H. R. Schober, Phys. Rev. B **67**, 094203 (2003).
[10] H. R. Schober and B. B. Laird, Phys. Rev. B **44**, 6746 (1991).
[11] V. Mazzacurati, G. Ruocco, and M. Sampoli, Europhys. Lett. **34**, 681 (1996).
[12] H. R. Schober and G. Ruocco, Philos. Mag. **84**, 1361 (2004).
[13] P. Derlet, R. Maaß, and J. Löffler, Eur. Phys. J. B **85**, 148 (2012).
[14] S. N. Taraskin and S. R. Elliott, Phys. Rev. B **59**, 8572 (1999).
[15] Y. M. Beltukov, C. Fusco, D. A. Parshin, and A. Tanguy, Phys. Rev. E **93**, 023006 (2016).
[16] N. Xu, V. Vitelli, A. J. Liu, and S. R. Nagel, Europhys. Lett. **90**, 56001 (2010).
[17] M. Baity-Jesi, V. Martín-Mayor, G. Parisi, and S. Perez-Gaviro, Phys. Rev. Lett. **115**, 267205 (2015).
[18] E. Lerner, G. Düring, and E. Bouchbinder, Phys. Rev. Lett. **117**, 035501 (2016).
[19] L. Gartner and E. Lerner, Phys. Rev. E **93**, 011001 (2016).
[20] H. Mizuno, H. Shiba, and A. Ikeda, Proc. Natl. Acad. Sci. USA **114**, E9767 (2017).
[21] M. Shimada, H. Mizuno, and A. Ikeda, Phys. Rev. E **97**, 022609 (2018).
[22] V. Gurarie and J. T. Chalker, Phys. Rev. B **68**, 134207 (2003).
[23] E. Bouchbinder and E. Lerner, New J. Phys. **20**, 073022 (2018).
[24] E. Lerner and E. Bouchbinder, Phys. Rev. E **97**, 032140 (2018).
[25] C. E. Maloney and A. Lemaitre, Phys. Rev. E **74**, 016118 (2006).
[26] A. Tanguy, B. Mantisi, and M. Tsamados, Europhys. Lett. **90**, 16004 (2010).
[27] M. L. Manning and A. J. Liu, Phys. Rev. Lett. **107**, 108302 (2011).
[28] C. Oligschleger and H. R. Schober, Phys. Rev. B **59**, 811 (1999).
[29] A. Widmer-Cooper, H. Perry, P. Harrowell, and D. R. Reichman, J. Chem. Phys. **131**, 194508 (2009).
[30] E. Lerner and E. Bouchbinder, J. Chem. Phys. **148**, 214502 (2018).
[31] C. S. O'Hern, S. A. Langer, A. J. Liu, and S. R. Nagel, Phys. Rev. Lett. **88**, 075507 (2002).
[32] C. S. O'Hern, L. E. Silbert, A. J. Liu, and S. R. Nagel, Phys. Rev. E **68**, 011306 (2003).
[33] L. E. Silbert, A. J. Liu, and S. R. Nagel, Phys. Rev. Lett. **95**, 098301 (2005).
[34] M. Wyart, S. R. Nagel, and T. A. Witten, Europhys. Lett. **72**, 486 (2005).
[35] M. Wyart, L. E. Silbert, S. R. Nagel, and T. A. Witten, Phys. Rev. E **72**, 051306 (2005).
[36] L. E. Silbert, A. J. Liu, and S. R. Nagel, Phys. Rev. E **79**, 021308 (2009).
[37] M. van Hecke, J. Phys.: Condens. Matter **22**, 033101 (2010).
[38] M. Wyart, Europhys. Lett. **89**, 64001 (2010).
[39] A. Ikeda, L. Berthier, and G. Biroli, J. Chem. Phys. **138**, 12A507 (2013).
[40] E. DeGiuli, A. Laversanne-Finot, G. During, E. Lerner, and M. Wyart, Soft Matter **10**, 5628 (2014).
[41] P. Charbonneau, E. I. Corwin, G. Parisi, A. Poncet, and F. Zamponi, Phys. Rev. Lett. **117**, 045503 (2016).
[42] H. Mizuno, K. Saitoh, and L. E. Silbert, Phys. Rev. E **93**, 062905 (2016).
[43] L. Yan, E. DeGiuli, and M. Wyart, Europhys. Lett. **114**, 26003 (2016).
[44] E. Bitzek, P. Koskinen, F. Gähler, M. Moseler, and P. Gumbsch, Phys. Rev. Lett. **97**, 170201 (2006).
[45] S. Alexander, Phys. Rep. **296**, 65 (1998).
[46] V. A. Luchnikov, N. N. Medvedev, Y. I. Naberukhin, and H. R. Schober, Phys. Rev. B **62**, 3181 (2000).
[47] W. G. Ellenbroek, M. van Hecke, and W. van Saarloos, Phys. Rev. E **80**, 061307 (2009).
[48] A. Heuer and R. J. Silbey, Phys. Rev. B **53**, 609 (1996).
[49] E. Cerda and L. Mahadevan, Phys. Rev. Lett. **90**, 074302 (2003).
[50] G. Düring, E. Lerner, and M. Wyart, Soft Matter **9**, 146 (2013).
[51] E. Lerner, E. DeGiuli, G. During, and M. Wyart, Soft Matter **10**, 5085 (2014).
[52] K. Karimi and C. E. Maloney, Phys. Rev. E **92**, 022208 (2015).
[53] N. Xu, M. Wyart, A. J. Liu, and S. R. Nagel, Phys. Rev. Lett. **98**, 175502 (2007).
[54] J. Phillips, J. Non-Cryst. Solids **34**, 153 (1979).
[55] L. Wang, A. Ninarello, P. Guan, L. Berthier, G. Szamel, and E. Flenner, Low-frequency vibrational modes of stable glasses, arXiv:1804.08765.